Efficiency Maximization of Wireless Power Transfer Based on Simultaneous Estimation of Primary Voltage and Mutual Inductance Using Secondary-Side Information

Katsuhiro Hata, Takehiro Imura, and Yoichi Hori
The University of Tokyo
5–1–5, Kashiwanoha, Kashiwa, Chiba, 277–8561, Japan
Phone: +81-4-7136-3881, Fax: 81-4-7136-3881
Email: hata@hflab.k.u-tokyo.ac.jp, imura@hori.k.u-toyko.ac.jp, hori@k.u-tokyo.ac.jp

***Abstract*—A dynamic wireless charging system for electric vehicles (EVs) is expected to extend the limited driving distance of EVs. As the transmitting efficiency changes according to motion of the vehicle in dynamic charging, an efficiency maximization method is important. Previous research has proposed secondary-side efficiency control based on mutual inductance estimation to simplify the ground facilities, which would be installed over long distances. However, the ground facilities have to regulate the primary voltage to achieve maximum efficiency control on the secondary side without signal communication. In this paper, a calculation method of the reference value for maximum efficiency control is proposed using simultaneous estimation of the primary voltage and the mutual inductance on the secondary side to eliminate the need for the primary voltage regulation. Simulations and experiments demonstrate that the proposed method is available for maximum efficiency control on the secondary side.**

***Keywords*—Wireless power transfer, Magnetic resonance, Electric vehicle, Parameter estimation, Secondary-side control**

I. Introduction

Wireless power transfer (WPT) has gathered attention in recent years for transportation applications [1]–[3]. Eliminating the use of wiring not only simplifies charging operations but also reduces the risk of accidents such as electric shock, disconnecting, and so on. In addition, a dynamic wireless charging system for electric vehicles (EVs) can extend the limited driving distance of EVs and reduce the size of the energy storage system of EVs [4], [5].

WPT via magnetic resonance coupling [6] has many advantages such as a highly efficient transmission, robustness to misalignment, and so on. Although these are feasible characteristics for dynamic charging of EVs, the transmitting efficiency is determined according to the load condition and the mutual inductance between the transmitter and receiver [7]. Consequently, it is an important issue to achieve the maximum efficiency regardless of the vehicle motion. However, the ground facilities, which consist of transmitters, inverters, and so on, should be simply designed because they would be installed over long distances. Therefore, secondary-side control is preferable to primary-side control [8] or dual-side control [9] to reduce the complexity of the ground facilities.

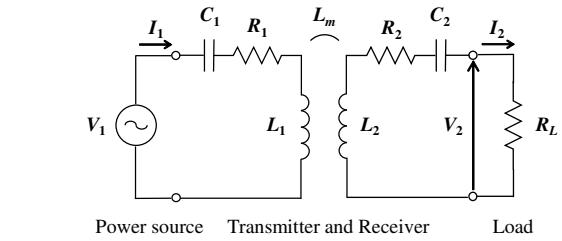

(a) Equivalent circuit of magnetic resonance coupling.

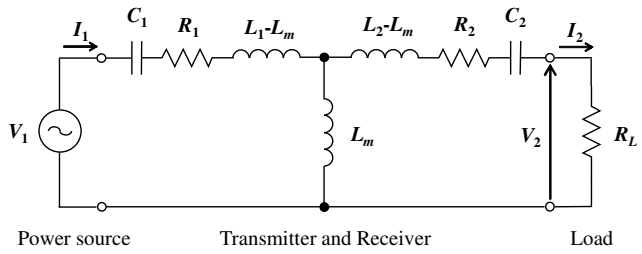

(b) T-type equivalent circuit.

Fig. 1. Equivalent circuit of the wireless power transfer system.

Although previous research has proposed maximum efficiency control based on mutual inductance estimation from the secondary side [10], [11], the primary voltage has to be regulated by the ground facilities. If the primary voltage and the mutual inductance are simultaneously estimated from the secondary side, the ground facilities can be further simplified. Although primary-side multi-parameter estimation has been proposed [12], this paper uses multi-parameter estimation from the secondary side using power converters for secondary-side control [13].

In this paper, maximum efficiency control based on simultaneous estimation of the primary voltage and the mutual inductance using secondary-side information is proposed. Then, the reference voltage for efficiency maximization is calculated from the estimated values. Simulations and experiments demonstrate the effectiveness of the proposed method.

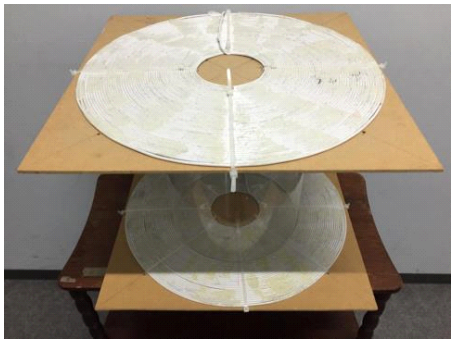

Fig. 2. Transmitter and receiver coils.

TABLE I. SPECIFICATIONS OF COILS.

	Primary side	Secondary side
Resistance R_1, R_2	1.19 Ω	1.23 Ω
Inductance L_1, L_2	617 μH	617 μH
Capacitance C_1, C_2	4000 pF	4000 pF
Resonance frequency f_1, f_2	101.3 kHz	101.3 kHz
Mutual inductance L_m	37.3 μH (Gap: 300 mm)	
	77.8 μH (Gap: 200 mm)	
Coupling coefficient k	0.060 (Gap: 300 mm)	
	0.126 (Gap: 200 mm)	
Outer diameter	440 mm	
Number of turns	50 turns	

II. WIRELESS POWER TRANSFER VIA MAGNETIC RESONANCE COUPLING

A. Characteristics at resonance frequency

This paper uses a series-series (SS) compensated circuit topology of WPT via magnetic resonance coupling. Its circuit diagram is shown in Fig. 1 [14]. V_1 is the RMS value of the primary voltage and R_L is the load resistance. The transmitter and receiver are composed of the coils and the series-resonant capacitors, which are characterized by the internal resistances R_1, R_2, the inductances L_1, L_2, and the capacitances C_1, C_2, respectively. L_m is the mutual inductance between the transmitter and receiver. The power source angular frequency ω_0 is designed as follows:

$$\omega_0 = \frac{1}{\sqrt{L_1 C_1}} = \frac{1}{\sqrt{L_2 C_2}}. \tag{1}$$

From the circuit equations, the voltage ratio A_V and the current ratio A_I between the primary side and the secondary side are described as follows:

$$A_V = \frac{V_2}{V_1} = \frac{\omega_0 L_m R_L}{R_1(R_2 + R_L) + (\omega_0 L_m)^2} \tag{2}$$

$$A_I = \frac{I_2}{I_1} = \frac{\omega_0 L_m}{R_2 + R_L} \tag{3}$$

where V_2, I_1, and I_2 are the RMS values of the secondary voltage, the primary current, and the secondary current, respectively. Then, the transmitting efficiency η is given as follows:

$$\eta = \frac{(\omega_0 L_m)^2 R_L}{(R_2 + R_L)\{R_1(R_2 + R_L) + (\omega_0 L_m)^2\}}. \tag{4}$$

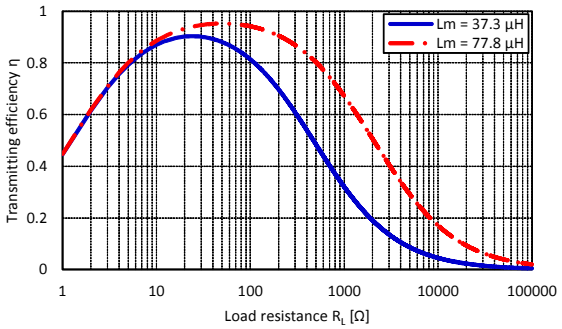

Fig. 3. Load resistance R_L vs. transmitting efficiency η.

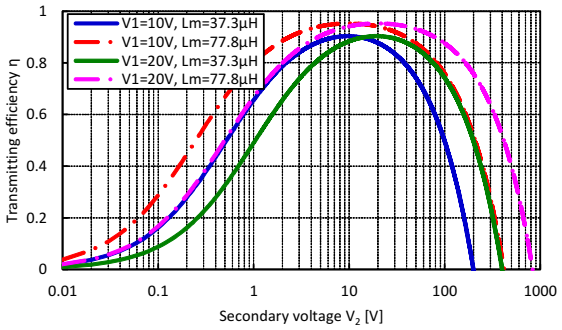

Fig. 4. Secondary voltage V_2 vs. transmitting efficiency η.

B. Maximization of transmitting efficiency

Fig. 2 shows the transmitter and receiver, which are used in this study, and their parameters are expressed in TABLE I. Then, Fig. 3 shows the load resistance R_L versus the transmitting efficiency η. For efficiency maximization, the load resistance R_L has to be given as follows [7]:

$$R_{L\eta\max} = \sqrt{R_2 \left\{ \frac{(\omega_0 L_m)^2}{R_1} + R_2 \right\}}. \tag{5}$$

Since eq. (5) does not include the primary voltage V_1, $R_{L\eta\max}$ is determined only by the mutual inductance L_m.

If the primary voltage V_1 is given, the transmitting efficiency η can be maximized by secondary voltage control [10], [11]. Fig. 4 shows the secondary voltage V_2 versus the transmitting efficiency η. From eq. (2) and eq. (5), the secondary voltage $V_{2\eta\max}$, which maximizes the transmitting efficiency η, is obtained as follows [10]:

$$V_{2\eta\max} = \sqrt{\frac{R_2}{R_1}} \frac{\omega_0 L_m}{\sqrt{R_1 R_2 + (\omega_0 L_m)^2} + \sqrt{R_1 R_2}} V_1. \tag{6}$$

Therefore, maximum efficiency control can be achieved by secondary voltage control. However, $V_{2\eta\max}$ is determined not only by L_m but also by V_1.

C. System configuration

The circuit diagram of the WPT system is shown in Fig. 5. The power source consists of the DC voltage source and the inverter, which generates a square voltage with the resonance angular frequency ω_0. Half Active Rectifier (HAR) is used as

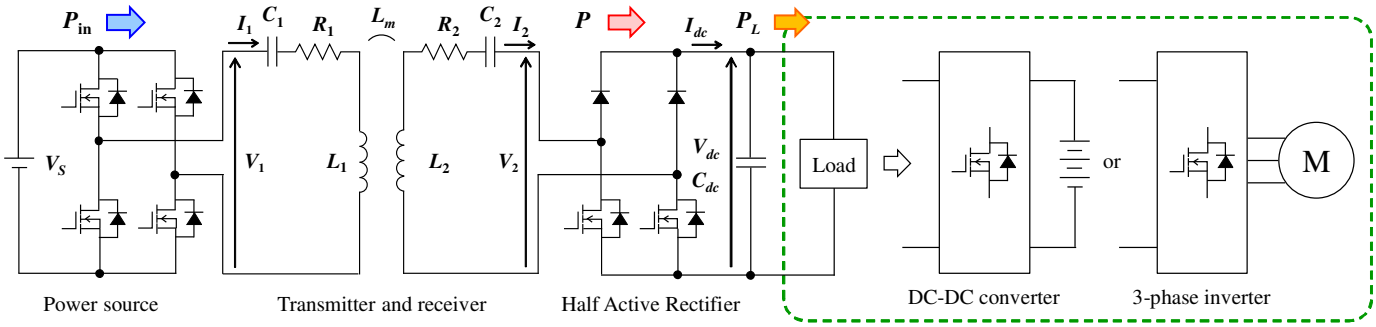

Fig. 5. Circuit diagram of the wireless power transfer system using Half Active Rectifier.

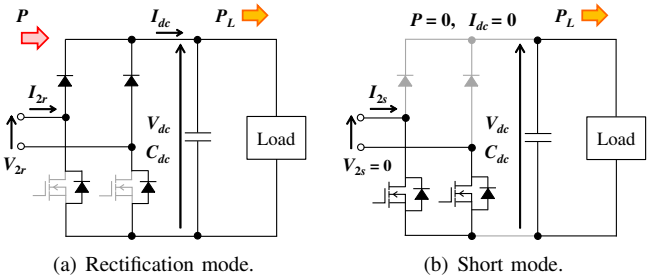

(a) Rectification mode. (b) Short mode.

Fig. 6. Operation modes of Half Active Rectifier.

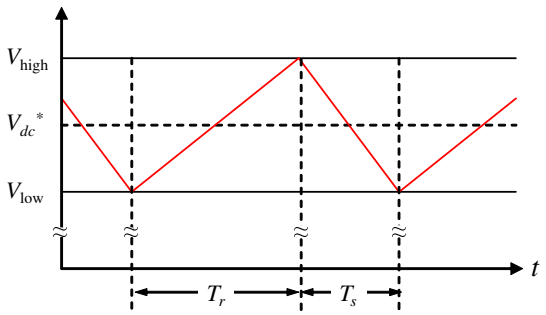

Fig. 7. Waveform of DC link voltage by HAR control.

an AC-DC converter and composed of the upper arm diodes and the lower arm MOSFETs. The DC link voltage V_{dc} is controlled by the HAR to achieve secondary voltage control for efficiency maximization. The load is assumed to be a battery charging system or a motor drive system, which include power converters for power control.

D. Secondary voltage control by Half Active Rectifier

HAR controls the DC link voltage V_{dc} using two operation modes, which are shown in Fig. 6. The rectification mode has the same function as the diode rectifier. Then, the lower arm MOSFETs are off state and the transmitting power P flows into the DC link capacitor. If P is larger than the load power P_L, V_{dc} is increased during the rectification mode. On the other hand, the short mode is worked by turning on the lower arm MOSFETs and P is cut-off. As a result, V_{dc} is decreased during the short mode.

Fig. 7 shows the waveform of V_{dc} in the case of HAR control with hysteresis comparator [3]. The upper bound $V_{\rm high}$ and the lower bound $V_{\rm low}$ are defined as follows:

$$V_{\rm high} = V_{dc}{}^* + \Delta V \tag{7}$$
$$V_{\rm low} = V_{dc}{}^* - \Delta V, \tag{8}$$

where $V_{dc}{}^*$ is the reference voltage and ΔV is the hysteresis band. Fig. 7 shows that V_{dc} can be kept within the desired range by switching the operation modes of HAR.

Assuming losses during the short mode is negligible to losses during the rectification mode, the transmitting efficiency has to be maximized during the rectification mode. From eq. (6), $V_{dc}{}^*$ has to be set to $V_{dc\eta\max}$, which is given as follows:

$$V_{dc\eta\max} = \sqrt{\frac{R_2}{R_1}} \frac{\omega_0 L_m}{\sqrt{R_1 R_2 + (\omega_0 L_m)^2} + \sqrt{R_1 R_2}} V_1. \tag{9}$$

where V_1 is the RMS value of the square voltage, which is generated by the inverter. Consequently, $V_{dc\eta\max}$ is calculated considering Fourier series expansions.

III. Parameter Estimation and Reference Calculation Using Secondary-Side Information

A. Conventional estimation method

1) Secondary current: Previous research has proposed the estimation method of the primary voltage V_1 [15] or the mutual inductance L_m [11] based on the secondary current of the WPT system. When a diode rectifier is used in the secondary side, the RMS secondary current I_2 is expressed as follows:

$$I_2 \simeq \frac{\omega_0 L_m V_{11} - R_1 V_{21}}{R_1 R_2 + (\omega_0 L_m)^2} = \frac{2\sqrt{2}}{\pi} \frac{\omega_0 L_m V_1 - R_1 V_2}{R_1 R_2 + (\omega_0 L_m)^2} \tag{10}$$

where V_{11} and V_{21} are the RMS values of the fundamental primary and secondary voltages. They are calculated from the RMS values of the primary voltage V_1 and the secondary voltage V_2 using Fourier series expansions. Since V_2 and I_2 can be measured on the secondary side, eq. (10) can be applied to V_1 and L_m estimation.

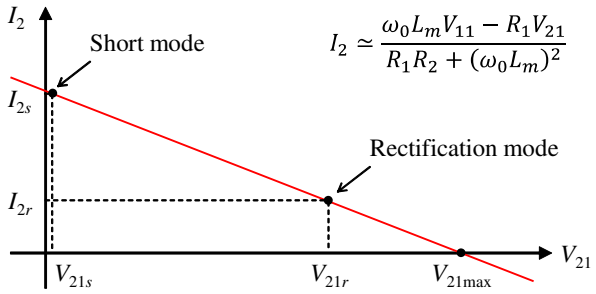

Fig. 8. Secondary current I_2 in each operation modes of HAR.

2) Primary voltage and mutual inductance estimation: If L_m is assumed to be constant and given, the fundamental primary voltage V_{11} can be estimated as follows [15]:

$$\hat{V}_{11} = \frac{R_1 V_{21} + \left\{R_1 R_2 + (\omega_0 L_m)^2\right\} I_2}{\omega_0 L_m}. \tag{11}$$

Assuming the primary voltage is a square wave, $\hat{V}_1$ can be obtained in the same way.

If V_1 is regulated by the primary-side ground facilities, L_m can be estimated as follows [11]:

$$\hat{L}_m = \frac{V_{11} \pm \sqrt{{V_{11}}^2 - 4R_1 I_2 (V_{21} + R_2 I_2)}}{2\omega_0 I_2}. \tag{12}$$

Although eq. (12) has two solutions, the solution with a positive sign is used considering the system condition.

These estimations cannot be achieved simultaneously because the estimation equation is given by the analysis of the WPT circuit for steady state. The conventional WPT system, which uses a diode rectifier instead of HAR, has only the rectification mode and the persistently exciting condition cannot be satisfied.

B. Multi-parameter estimation method [13]

1) Operation modes of HAR: HAR is operated in two different modes for secondary-side control. From eq. (10), the secondary current I_2 is expressed as a linear function of the fundamental secondary voltage V_{21}. Since V_{21} and I_2 can be obtained in each operation modes as shown in Fig. 8, simultaneous estimation of two parameters can be achieved. This paper focuses on the primary voltage V_1 and the mutual inductance L_m. Their estimation method is derived from eq. (10).

2) Simultaneous estimation of primary voltage and mutual inductance: Firstly, unknown parameters are distinguish from measurable parameters. Eq. (10) is transformed as follows:

$$\omega_0 L_m V_{11} - I_2 (\omega_0 L_m)^2 = R_1 (V_{21} + R_2 I_2). \tag{13}$$

Then, the estimation equation is given as follows:

$$x_1 - I_2 x_2 = R_1 (V_{21} + R_2 I_2) \tag{14}$$

$$\boldsymbol{x} = \begin{bmatrix} x_1 & x_2 \end{bmatrix}^T := \begin{bmatrix} \omega_0 L_m V_{11} & (\omega_0 L_m)^2 \end{bmatrix}^T. \tag{15}$$

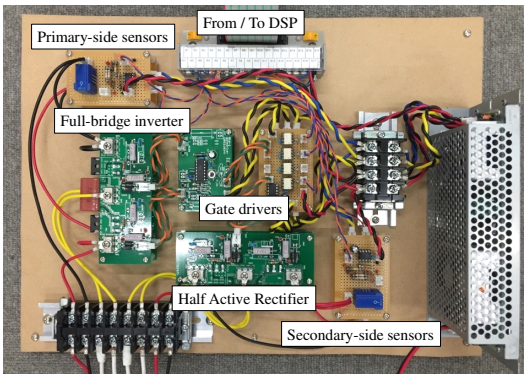

Fig. 9. Experimental equipment.

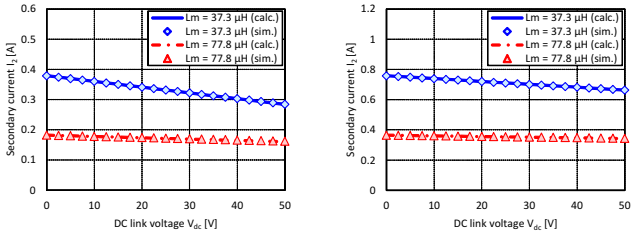

(a) $V_1 = 10$ V. (b) $V_1 = 20$ V.

Fig. 10. Experimental results of the secondary current I_2.

Therefore, estimated parameter $\hat{\boldsymbol{x}}$ can be obtained as follows:

$$\hat{\boldsymbol{x}} = \begin{bmatrix} \hat{x}_1 & \hat{x}_2 \end{bmatrix}^T = \boldsymbol{A}^{-1}\boldsymbol{b} \tag{16}$$

$$\boldsymbol{A} := \begin{bmatrix} 1 & -I_{2r} \\ 1 & -I_{2s} \end{bmatrix}, \ \boldsymbol{b} := \begin{bmatrix} R_1(V_{21r} + R_2 I_{2r}) \\ R_1(V_{21s} + R_2 I_{2s}) \end{bmatrix}$$

where I_{2r}, V_{21r}, I_{2s}, and V_{21s} are the measured values of I_2 and V_{21} during the rectification mode and during the short mode.

Assuming that the secondary voltage is a square wave and the voltage drop of the MOSFETs is negligible, V_{21r} and V_{21s} are calculated as follows:

$$V_{21r} = \frac{2\sqrt{2}}{\pi} V_{2r} = \frac{2\sqrt{2}}{\pi}(V_{dc} + 2V_f) \tag{17}$$

$$V_{21s} = \frac{2\sqrt{2}}{\pi} V_{2s} = 0 \tag{18}$$

where V_f is the forward voltage of the diodes. From eq. (15) and eq. (16), the mutual inductance $\hat{L}_m$ and the primary voltage $\hat{V}_1$ can be estimated as follows:

$$\hat{L}_m = \frac{1}{\omega_0}\sqrt{\hat{x}_2} \tag{19}$$

$$\hat{V}_1 = \frac{\pi}{2\sqrt{2}}\hat{V}_{11} = \frac{\pi}{2\sqrt{2}}\frac{\hat{x}_1}{\omega_0 \hat{L}_m}. \tag{20}$$

C. Reference voltage calculation

The reference voltage $V_{dc\eta\max}$ for maximum efficiency control can be calculated from eq. (9), eq. (19), and eq. (20). By controlling V_{dc} to $V_{dc\eta\max}$, the transmitting efficiency can be maximized from the secondary-side.

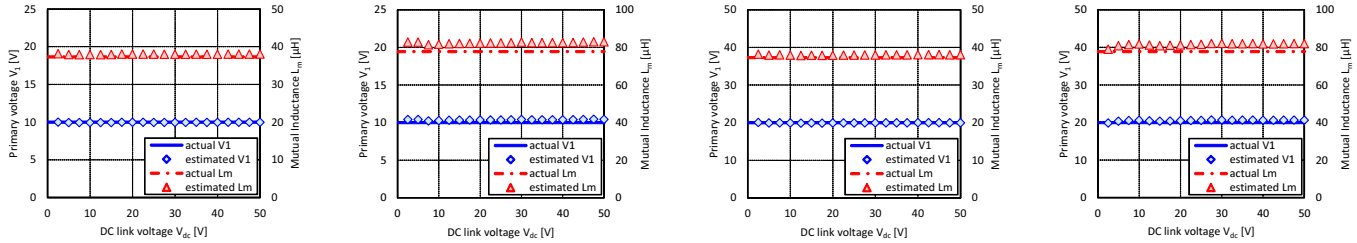

(a) $V_1 = 10$ V, $L_m = 37.3$ μH. (b) $V_1 = 10$ V, $L_m = 77.8$ μH. (c) $V_1 = 20$ V, $L_m = 37.3$ μH. (d) $V_1 = 20$ V, $L_m = 77.8$ μH.

Fig. 11. Simulation results of the primary voltage V_1 and the mutual inductance L_m estimation.

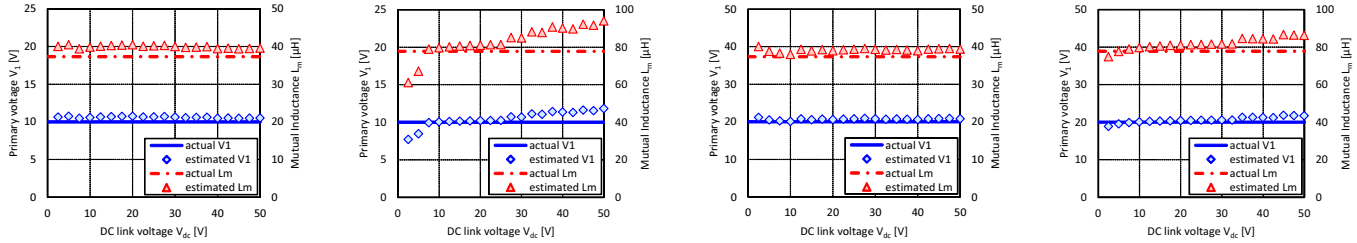

(a) $V_1 = 10$ V, $L_m = 37.3$ μH. (b) $V_1 = 10$ V, $L_m = 77.8$ μH. (c) $V_1 = 20$ V, $L_m = 37.3$ μH. (d) $V_1 = 20$ V, $L_m = 77.8$ μH.

Fig. 12. Experimental results of the primary voltage V_1 and the mutual inductance L_m estimation.

IV. Simulation and Experiment

A. Experimental equipment and conditions

The effectiveness of the proposed method was verified by simulations and experiments. The circuit configuration is shown in Fig. 5 and the power converters are shown in Fig. 9. The power source was composed of a DC power supply (ZX-400LA, TAKASAGO) and the full-bridge inverter, which generated a square wave voltage with the resonance frequency of the transmitter and receiver. The inverter and the HAR were controlled by a DSP (PE-PRO/F28335A, Myway). The load was simulated by an electronic load (PLZ1004W, KIKUSUI) and the DC link voltage V_{dc} was regulated by the electronic load instead of HAR control.

The amplitude of the primary voltage V_1 was tuned to 10 V and 20 V. The transmitting distance was set to 200 mm and 300 mm. The load was assumed to be a constant voltage and its amplitude V_{dc} was gradually increased in 2.5 V increments from 2.5 V to 50 V during simulations and experiments.

The RMS secondary current I_2 was measured by a digital phosphor oscilloscope (DPO2024, Tektronix). Fig. 10 compares the measured values of secondary current I_2 with their actual values. As they are closely matched, eq. (10) can be applied to the estimation method from the secondary-side.

B. Simultaneous estimation of primary voltage and mutual inductance

Simulation results of V_1 and L_m estimation are shown in Fig. 11. Although the estimated primary voltage in Fig. 11(b) and Fig. 11(d) are slightly larger than these actual values, the estimated values are roughly the same as the actual values.

Fig. 12 shows experimental results of V_1 and L_m estimation. From these results, the reduction of the estimation accuracy is confirmed. Especially, Fig. 12(b) is the worst case because I_2 during the short mode is nearly unchanged from the one during the rectification mode in a low V_1 and high L_m condition. As a result, a resolution capability of the current measurement has to be improved for the accurate estimation. However, Fig. 12(c) indicates that the estimated values are close to the actual values. Consequently, high power and low coupling application such as dynamic charging of EVs is more suitable for the proposed estimation method.

C. Reference voltage calculation and efficiency maximization

Fig. 13 shows the simulation results of the reference voltage calculation for efficiency maximization based on simultaneous estimation of V_1 and L_m. From Fig. 13(a) and Fig. 13(c), the estimated reference voltage $\hat{V}_{dc\eta\max}$ can be obtained using $\hat{V}_1$ and $\hat{L}_m$, which are shown in Fig. 11, regardless of the simulation condition. Although the transmitting efficiency η changes according to V_{dc} as shown in Fig. 13(b) and Fig. 13(d), η can be maximized by controlling V_{dc} to $\hat{V}_{dc\eta\max}$.

The experimental results of the reference voltage calculation are shown in Fig. 14(a) and Fig. 14(c). As the experimental results of $\hat{V}_1$ and $\hat{L}_m$ are poorly matched compared to the simulation results, $\hat{V}_{dc\eta\max}$ is slightly different from the actual value $V_{dc\eta\max}$. However, the proposed method is effective for maximum efficiency control of the WPT system because Fig. 14(b) and Fig. 14(d) demonstrate that η can be much-improved using $\hat{V}_{dc\eta\max}$ as the reference voltage. If the forward voltage of HAR is compensated, the estimation accuracy is improved and η becomes fairly close to the maximum value.

V. Conclusion

This paper proposed a reference voltage calculation method for efficiency maximization from the secondary side in a

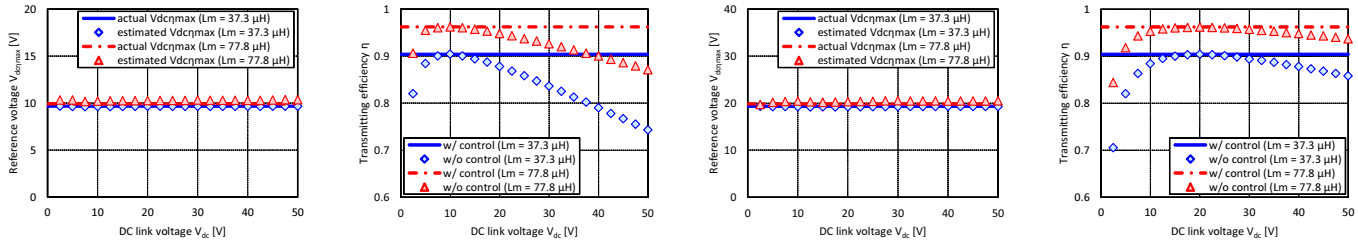

(a) $\hat{V}_{dc\eta\max}$ ($V_1 = 10$ V). (b) η ($V_1 = 10$ V). (c) $\hat{V}_{dc\eta\max}$ ($V_1 = 10$ V). (d) η ($V_1 = 20$ V).

Fig. 13. Simulation results of reference voltage calculation for efficiency maximization.

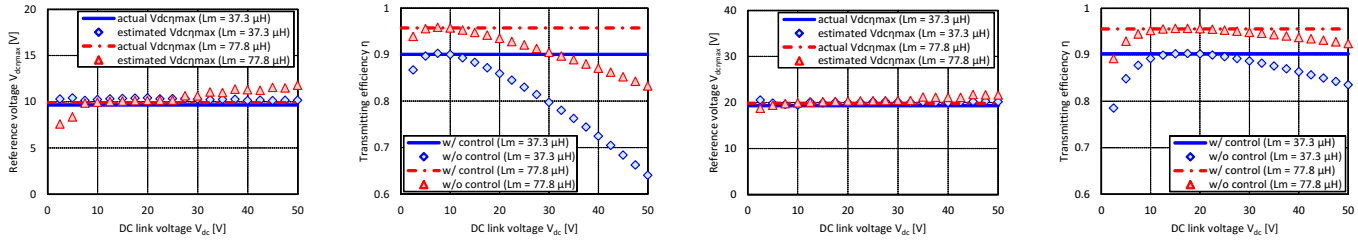

(a) $\hat{V}_{dc\eta\max}$ ($V_1 = 10$ V). (b) η ($V_1 = 10$ V). (c) $\hat{V}_{dc\eta\max}$ ($V_1 = 20$ V). (d) η ($V_1 = 20$ V).

Fig. 14. Experimental results of reference voltage calculation for efficiency maximization.

WPT system using simultaneous estimation of the primary voltage and the mutual inductance based on the operation modes of HAR. Simulations and experiments demonstrated the effectiveness of maximum efficiency control based on the proposed method.

Future works are to implement maximum efficiency control using the proposed method and to apply the proposed control strategy to a dynamic WPT system.

ACKNOWLEDGMENTS

This work was partly supported by JSPS KAKENHI Grant Number 25709020 and 15H02232.

REFERENCES

[1] G. A. Covic and J. T. Boys, "Modern trends in inductive power transfer for transportation application," *IEEE Journal of Emerging and Selected Topics in Power Electronics*, vol. 1, no.1, pp. 28–41, Mar. 2013.

[2] S. Li and C. C. Mi, "Wireless power transfer for electric vehicle applications," *IEEE Journal of Emerging and Selected Topics in Power Electronics*, vol. 3, no.1, pp. 4–17, Mar. 2015.

[3] D. Gunji, T. Imura, and H. Fujimoto, "Basic study of transmitting power control method without signal communication for wireless in-wheel motor via magnetic resonance coupling," in *Proc. IEEE/IES International Conference on Mechatronics*, 2015, pp. 313–318.

[4] J. Shin, S. Shin, Y. Kim, S. Ahn, S. Lee, G. Jung, S. Jeon, and D. Cho, "Design and implementation of shaped magnetic-resonance-based wireless power transfer system for roadway-powered moving electric vehicles," *IEEE Transactions on Industrial Electronics*, vol. 61, no. 3, pp. 1179–1192, Mar. 2014.

[5] J. M. Miller, O. C. Onar, C. White, S. Campbell, C. Coomer, L. Seiber, R. Sepe, and M. Chinthavali, "Demonstrating dynamic charging of an electric vehicle: the benefit of electrochemical capacitor smoothing," *IEEE Power Electronics Magazine*, vol. 1, no.1, pp. 12–24, Mar. 2014.

[6] A. Kurs, A. Karalis, R. Moffatt, J. D. Joannopoulos, P. Fisher, and M. Soljacic, "Wireless power transfer via strongly coupled magnetic resonance," *Science Express on 7 June 2007*, vol. 317, no. 5834, pp. 83–86, Jun. 2007.

[7] M. Kato, T. Imura, and Y. Hori, "New characteristics analysis considering transmission distance and load variation in wireless power transfer via magnetic resonant coupling," in *Proc. IEEE 34th International Telecommunications Energy Conference*, 2012, pp. 1–5.

[8] J. M. Miller, O. C. Onar, and M. Chinthavali, "Primary-side power flow control of wireless power transfer for electric vehicle charging," *IEEE Journal of Emerging and Selected Topics in Power Electronics*, vol. 3, no.1, pp. 147–162, Mar. 2015.

[9] H. H. Wu, A. Gilchrist, K. D. Sealy, and D. Bronson, "A high efficiency 5 kW inductive charger for EVs using dual side control," *IEEE Transactions on Industrial Informatics*, vol. 8, no. 3, pp. 585–595, Aug. 2012.

[10] M. Kato, T. Imura, and Y. Hori, "Study on maximize efficiency by secondary side control using DC-DC converter in wireless power transfer via magnetic resonant coupling," in *Proc. 27th International Electric Vehicle Symposium and Exhibition*, 2013, pp. 1–5.

[11] D. Kobayashi, T. Imura, and Y. Hori, "Real-time coupling coefficient estimation and maximum efficiency control on dynamic wireless power transfer for electric vehicles," in *Proc. IEEE PELS Workshop on Emerging Technologies; Wireless Power*, 2015, pp. 1–6.

[12] J. P. W. Chow and H. S. H. Chung, "Use of primary-side information to perform online estimation of the secondary-side information and mutual inductance in wireless inductive link," in *Proc. 30th Annual IEEE Applied Power Electronics Conference and Exposition*, 2015, pp. 2648–2655.

[13] K. Hata, T. Imura, and Y. Hori, "Simultaneous estimation of primary voltage and mutual inductance based on secondary-side information in wireless power transfer systems," in *Proc. IEEE MTT-S Wireless Power Transfer Conference*, 2016, pp. 1–6.

[14] T. Imura and Y. Hori, "Maximizing air gap and efficiency of magnetic resonant coupling for wireless power transfer using equivalent circuit and Neumann formula," *IEEE Transactions on Industrial Electronics*, vol. 58, no. 10, pp. 4746–4752, Oct. 2011.

[15] K. Hata, T. Imura, and Y. Hori, "Dynamic wireless power transfer system for electric vehicle to simplify ground facilities - power control based on vehicle-side information -," in *Proc. 28th International Electric Vehicle Symposium and Exhibition*, 2015, pp. 1–12.